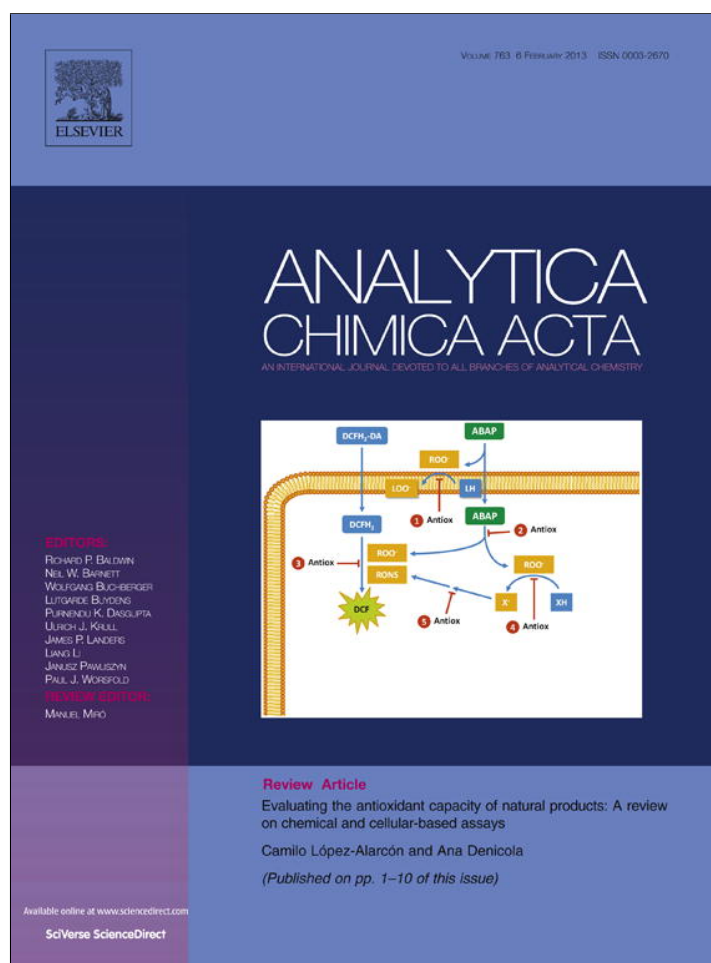


Provided for non-commercial research and education use.  
Not for reproduction, distribution or commercial use.



This article appeared in a journal published by Elsevier. The attached copy is furnished to the author for internal non-commercial research and education use, including for instruction at the authors institution and sharing with colleagues.

Other uses, including reproduction and distribution, or selling or licensing copies, or posting to personal, institutional or third party websites are prohibited.

In most cases authors are permitted to post their version of the article (e.g. in Word or Tex form) to their personal website or institutional repository. Authors requiring further information regarding Elsevier's archiving and manuscript policies are encouraged to visit:

<http://www.elsevier.com/copyright>



Contents lists available at SciVerse ScienceDirect

Analytica Chimica Acta

journal homepage: [www.elsevier.com/locate/aca](http://www.elsevier.com/locate/aca)

# Differentiation and characterization of isotopically modified silver nanoparticles in aqueous media using asymmetric-flow field flow fractionation coupled to optical detection and mass spectrometry



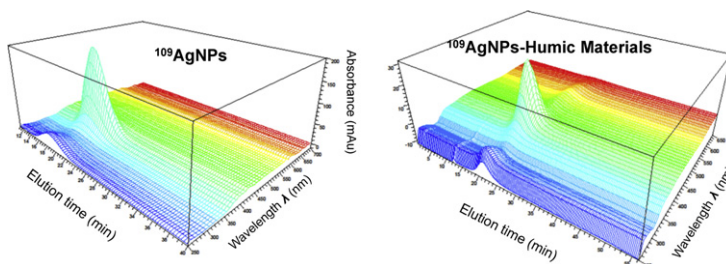
Julien Gigault, Vincent A. Hackley\*

National Institute of Standards and Technology, Material Measurement Laboratory, 100 Bureau Drive Stop 8520, Gaithersburg, MD 20899-8520, USA

## HIGHLIGHTS

- ▶ Isotopically modified and unmodified AgNPs characterization by A4F-DAD-MALS-DLS-ICP-MS.
- ▶ Size-resolved characterization and speciation in simple or complex media.
- ▶ Capacity to detect stable isotope enriched AgNPs in a standard estuarine sediment.
- ▶ New opportunities to monitor and study fate and transformations of AgNPs.

## GRAPHICAL ABSTRACT



## ARTICLE INFO

### Article history:

Received 4 September 2012

Received in revised form

28 November 2012

Accepted 30 November 2012

Available online 10 December 2012

### Keywords:

Field flow fractionation

Nanoparticles

Hyphenated techniques

Environmental monitoring

## ABSTRACT

The principal objective of this work was to develop and demonstrate a new methodology for silver nanoparticle (AgNP) detection and characterization based on asymmetric-flow field flow fractionation (A4F) coupled on-line to multiple detectors and using stable isotopes of Ag. This analytical approach opens the door to address many relevant scientific challenges concerning the transport and fate of nanomaterials in natural systems. We show that A4F must be optimized in order to effectively fractionate AgNPs and larger colloidal Ag particles. With the optimized method one can accurately determine the size, stability and optical properties of AgNPs and their agglomerates under variable conditions. In this investigation, we couple A4F to optical absorbance (UV–vis spectrometer) and scattering detectors (static and dynamic) and to an inductively coupled plasma mass spectrometer. With this combination of detection modes it is possible to determine the mass isotopic signature of AgNPs as a function of their size and optical properties, providing specificity necessary for tracing and differentiating labeled AgNPs from their naturally occurring or anthropogenic analogs. The methodology was then applied to standard estuarine sediment by doping the suspension with a known quantity of isotopically enriched  $^{109}\text{Ag}$  NPs stabilized by natural organic matter (standard humic and fulvic acids). The mass signature of the isotopically enriched AgNPs was recorded as a function of the measured particle size. We observed that AgNPs interact with different particulate components of the sediment, and also self-associate to form agglomerates in this model estuarine system. This work should have substantial ramifications for research concerning the environmental and biological fate of AgNPs.

Published by Elsevier B.V.

## 1. Introduction

Due principally to their antimicrobial properties, silver nanoparticles (AgNPs) have been increasingly exploited over the past decade for applications in industrial, biomedical and consumer

\* Corresponding author. Tel.: +1 301 975 5790.

E-mail address: [vince.hackley@nist.gov](mailto:vince.hackley@nist.gov) (V.A. Hackley).

products. Applications range from pesticides to coronary stents to self-deodorizing fabrics and even washing machines [1–11]. AgNPs are, in fact, the most commonly reported nanomaterial used in consumer products to-date, and have been available commercially for many years [12]. Ironically, the growing commercial interest in AgNPs has paralleled a growing public and regulatory anxiety as to the potential risks they may pose to the environment and to human health [13–18]. A recent surge in publications on the topic have shown that AgNPs are subject to dissolution, oxidation, sulfidation and other chemical and physical transformations that may impact their environmental fate and, ultimately, their risk assessment [13,14,19,20]. Much uncertainty remains regarding the hazards posed by AgNPs, due in part to their inherent chemical instability (the source of their antimicrobial activity via release of  $\text{Ag}^+$  ions), and a major challenge therefore exists for accurate and reproducible measurements [21–23]. Another primary source of uncertainty arises from the lack of proven analytical tools with the capacity to characterize and quantify AgNPs at environmentally relevant concentrations ( $\mu\text{g L}^{-1}$ ) and in complex environmental matrices that may induce polydisperse particle size distributions and contain interfering chemical and particulate species [24–27].

Regarding the scarcity of validated analytical tools for in situ high-sensitivity analysis, recent published studies have demonstrated promising potential for applying field flow fractionation to simultaneously separate and characterize AgNPs in aqueous media [28–32]. The A4F technique separates particles in an aqueous mobile phase based on their hydrodynamic properties in an applied cross-flow field, and can be utilized as a semi-preparative method for secondary analysis or hyphenated to various detection modes [33–36]. In the normal mode of operation for A4F, the smallest particles elute first and the elution time is linearly related to the diffusion coefficient of the particles. The coupling of this separative technique to different detectors, such as UV–vis absorbance, light scattering and inductively coupled plasma mass spectrometry (ICP–MS), enables the simultaneous determination of multi-dimensional particle parameters such as size, concentration and chemical composition. The multi-wavelength UV–vis detector (diode array detector, DAD) is particularly powerful for noble metal NPs, like Ag, that exhibit a surface plasmon resonance (SPR) effect [21,22,37], as the spectral absorbance can provide information on size, shape and concentration. Although recent studies have clearly demonstrated that the coupling of ICP–MS to A4F enables measurement of size-resolved elemental composition for AgNPs [28–30,32], the capacity to determine the association between AgNPs and other ions and particles or to discriminate between engineered AgNPs and anthropogenic or naturally occurring Ag colloids has not yet been established. Therefore, our ultimate goal is to develop a robust and standardized approach to detect, monitor and characterize AgNPs as they transport through natural (environmental or biological) systems with a high degree of specificity and sensitivity.

Beyond size-resolved elemental composition, coupling with ICP–MS also offers the possibility for precisely determining stable isotope mass ratios in speciation studies [38]. Nonetheless, to our knowledge, no study to-date has been published in which ICP–MS is directly interfaced to A4F and used to characterize isotopically enriched AgNPs. Indeed the combination of isotopic speciation with natural composition could open the door to applications for evaluating the environmental and biological fate of many technically challenging nanomaterials.

In the present work we propose a new methodology based principally on A4F coupled with UV–vis absorbance, multi-angle light scattering (MALS) and ICP–MS to characterize isotopically modified and unmodified AgNPs in order to obtain size-resolved characterization and speciation in both simple and complex media. We show that the method provides the capacity to detect isotopically enriched  $^{109}\text{Ag}$ NPs in a standard estuarine sediment

and to discriminate between isotopically enriched and other non-enriched AgNPs (e.g., commercial, natural or anthropogenic in nature) in natural media, and, finally, to investigate their interaction with other chemical species (e.g.,  $\text{Ag}^+$  ions).

## 2. Materials and methods

### 2.1. Reagents

Reagents used to formulate the mobile phase and to calibrate the ICP–MS were purchased from VWR (Philadelphia, PA)<sup>1</sup> as follows: ammonium nitrate ( $\text{NH}_4\text{NO}_3$ , >99%), high purity nitric acid ( $\text{HNO}_3$ , >99%) and silver standard ( $1000 \text{ mg L}^{-1}$  in 3%  $\text{HNO}_3$ , Ricca ICPMS NIST traceable standard.). Durapore 0.1  $\mu\text{m}$  filters (EMD Millipore, Billerica, MA) were used to remove particulates from the mobile phase. All solutions were prepared using ultrapure deionized water obtained from an Aqua Solutions (Jasper, GA) Type I biological grade purification system.

Silver nitrate with >99.0% purity was purchased from Sigma Aldrich (St. Louis, MO) and  $^{109}\text{Ag}$  isotope (99+ % enriched) in solid form was obtained from Trace Sciences International Inc. (Pilot Point, TX). Suwannee River Humic Acid Standard II and Suwannee River Fulvic Acid Standard I were purchased from the International Humic Substances Society (IHSS, St. Paul, MN). Trisodium citrate dihydrate and sodium borohydride were purchased from Sigma Aldrich. Citrate stabilized AgNPs in aqueous solution of nominal diameter 20 nm, 40 nm and 60 nm were obtained from Ted Pella, Inc. (Redding, CA). Nominally 100 nm PVP coated AgNPs were purchased from NanoComposix (San Diego, CA) with a stated concentration of  $0.02 \text{ g L}^{-1}$ . In order to calibrate retention time using A4F, polystyrene NPs (Thermo-scientific NIST traceable nanosphere size standards) were purchased from Fischer Scientific (Pittsburg, PA) as follows: 60 nm (#3060A), 100 nm (#3100A) and 150 nm (#3150A). Standard Reference Material (SRM) 1646a (Estuarine Sediment) was produced and certified by the National Institute of Standards and Technology; the certificate of analysis contains compositional data for this reference material [39].

### 2.2. Sample preparation

Citrate-stabilized AgNPs (isotopically enriched in  $^{109}\text{Ag}$  – denoted as  $^{109}\text{Ag}$ NPs – and with a natural isotopic ratio) were synthesized using a previously described method for reducing an aqueous solution of boiling silver nitrate in the presence of trisodium citrate dihydrate with sodium borohydride [40]. The final solutions were filtered by stirred cell with a 100 kDa molar mass cut-off regenerated cellulose filter. The supernatant was then re-suspended at the same initial volume. The only difference between the enriched and natural isotopic formulations is that the enriched  $^{109}\text{Ag}$  metal was first treated with nitric acid to obtain the nitrate salt.

AgNPs were coated with humic (HA) or fulvic (FA) acid by ligand exchange; AgNP suspensions were mixed with  $1 \text{ mmol L}^{-1}$  of either HA or FA at a 9:1 volume ratio, respectively, yielding a final HA or FA concentration of  $0.1 \text{ g L}^{-1}$ . The exchange was allowed to proceed for 24 h. The resulting suspensions were mildly acidic (pH 4.5–5.6).

To evaluate the quality and the applicability of the optimized methodology, an estuarine sediment leachate was prepared by mixing 1 g of SRM 1646a with 10 mL of an aqueous medium containing 30% (mass basis) AgNPs stabilized with HA ( $^{109}\text{AgNP-HA}$ ) or with FA ( $^{109}\text{AgNP-FA}$ ). The estuarine sediment leachate obtained

<sup>1</sup> The identification of any commercial product or trade name does not imply endorsement or recommendation by the National Institute of Standards and Technology.

by using  $^{109}\text{AgNP-HA}$  is identified in the text as S1 leachate, and the leachate obtained using  $^{109}\text{AgNP-FA}$  is identified as S2 leachate. In order to validate results, a control sample was produced, identified as leachate S0, by mixing the sediment with DI water containing no Ag, HA or FA, and the corresponding fractograms are presented in the supplemental information (SI, Fig. S4). The resulting preparations were agitated for 36 h, after which the mixture was centrifuged at  $2500 \times g$  for 5 min. Finally, the supernatant was collected and filtered at  $0.45 \mu\text{m}$ , and the pH adjusted to neutral prior to analysis. The pH of the control sample S0 was approximately 6.6 without adjustment. For all AgNPs synthesized in the current work the quantity of silver was determined and is detailed in the SI (see Section 3).

### 2.3. Instrumentation

The flow-mode analysis system used in this investigation consists of an Eclipse 3+ A4F (Wyatt Technology, Santa Barbara, CA), a 1200 series UV-vis absorbance DAD (Agilent Technologies, Santa Clara, CA), a multi-angle laser light scattering (MALS) detector (DAWN HELEOS, Wyatt Technology), and a dynamic light scattering (DLS) detector (DynaPro, Wyatt Technology). Data from the above detectors was collected and analyzed using Astra software version 5.3.1.18 (Wyatt Technology). The A4F channel height was established using spacers of  $250 \mu\text{m}$  or  $350 \mu\text{m}$  (optimized according to the nanoparticle size range – see Table 1). The channel dimensions are as follows:  $26.5 \text{ cm}$  long and narrowing in width from  $2.1 \text{ cm}$  or  $1.9 \text{ cm}$ , to  $0.6 \text{ cm}$ , for the  $350 \mu\text{m}$  or  $250 \mu\text{m}$  spacer, respectively. Polyethersulfone (PES)  $10 \text{ kDa}$  membranes were purchased from Wyatt Technology and used in the A4F cell. Mobile phase flow is generated using a 1200 series isocratic pump (Agilent Technologies) equipped with a degasser (Gastorr TG-14, Flom Co., Ltd., Tokyo, Japan). Injections are performed using a manual injection valve (Rheodyne 7725i, IDEX Corporation, Oak Harbor, WA) equipped with stainless steel sample loops of different volumes. The A4F and associated detection chain is coupled to a model 7700x ICP-MS (Agilent Technologies) with a Micro Mist nebulizer for quantitative mass determination. Off-line (batch mode) UV-vis absorbance and DLS measurements were performed using a Perkin Elmer (Waltham, MA) Lambda 750 spectrometer and a Malvern Instruments Inc. (Westborough, MA) ZetaSizer Nano, respectively. Further details regarding the instrumentation and techniques are provided in the SI.

### 2.4. Measurements

On-line DLS and MALS measurements by A4F with multi-mode on-line detection were conducted in a cell maintained at  $(20 \pm 0.1)^\circ\text{C}$ . Eluting samples were subject to ambient temperatures outside of the MALS cell, where the ambient temperature was generally within  $2^\circ\text{C}$  of the experimental temperature. Discrete measurement results are reported as the mean with an associated uncertainty of one standard deviation (presented as an interval or error bar) based on typically 3–5 replicates performed under repeatability conditions. A4F traces represent the mean of 3–5 replicate injections, where the average coefficient of variation between replicate elutions is less than 1%.

Isotopically enriched  $^{109}\text{AgNPs}$  and natural isotopic AgNPs were characterized via A4F by applying a previously developed optimization strategy described in the SI. Using this protocol, two optimal A4F fractionation methods were used to fractionate AgNPs and Ag colloids according to their size range. The conditions are summarized in Table 1 (column “condition A”).

Optimization addressed three primary A4F parameters: recovery, selectivity (peak resolving power) and linearity (size v.

retention ratio). These parameters and their respective calculations are described in Section 1 of the SI. Using the optimized conditions, the recovery based on the ICP-MS trace for each silver isotope, was calculated to exceed 90%. Size calibrations were realized using commercially available monodisperse citrate-stabilized AgNPs and polystyrene standards. Typical fractograms for this calibration procedure are also presented in the SI (see Fig. S1). Using these elution conditions (condition A, Table 1) it is possible to fractionate AgNPs at the highest achievable selectivity without compromising recovery. The calibration allows the hydrodynamic size ( $r_H$ ; nm) to be determined directly from the retention time ( $t_R$ ; min), where the corresponding relationship for fractionation condition A is:

$$r_H = 1.03 \cdot t_R - 0.26 \quad (R^2 = 0.990) \quad (1)$$

associated with a selectivity ( $S_d$ ) of  $0.74 \pm 0.04$ . For fractionation condition B the relationship is:

$$r_H = 5.24 \cdot t_R - 0.29 \quad (R^2 = 0.999) \quad (2)$$

associated with a  $S_d$  of  $0.99 \pm 0.01$ , where  $S_d = 1$  is the maximum attainable value.  $S_d$  is a measure of the ability of a chromatographic technique to separate two components (see SI, Section 1). The quantity  $t_R$  for a single population is determined at the maximum of the UV-vis peak (concentration detector) in a fractogram, and corresponds to the maximum concentration of the traced population at size  $r_H$ ;  $t_R$  is calculated from the elution time corresponding to the peak maximum after subtraction of the injection and focus times. The quality and validation of the A4F calibration is discussed in Section 3 of the main text. A  $100 \mu\text{L}$  injection of bulk solution was performed for each sample.

The radius of gyration ( $r_G$ ) and  $r_H$  were calculated using, respectively, the Zimm first-order fit formalism to MALS results obtained on-line and DLS ( $z$ -average size) where appropriate. Calibrated A4F retention time (as described above) was utilized to determine the  $r_H$  in the case of weak scattering signals and for polydisperse samples.

Coupling between the A4F detection train and the ICP-MS consists of a direct connection of the eluent exiting the MALS/DLS detector to the ICP-MS nebulizer, with a flow rate adjusted to maintain constant pressure inside the A4F channel. In this study, ICP-MS was operated without the collision cell, because of the lack of interferences for the two mass isotopes of interest ( $^{107}\text{Ag}$  and  $^{109}\text{Ag}$ ). The calibration of the ICP-MS was realized by placement of a six-way injection valve (Rheodyne 7725i, IDEX Corporation, Oak Harbor, WA) with a  $100 \mu\text{L}$  stainless steel sample loop between the MALS/DLS detector and the entrance of the ICP-MS nebulizer. For the calibration of the A4F-ICP-MS coupling, silver standard solutions (in 2% mass fraction of nitric acid) of various concentrations are injected ( $20 \mu\text{L}$ ) and replicated in order to have an accurate Ag mass quantification. All other parameters concerning the ICP-MS are summarized in Table 1.

## 3. Results and discussion

### 3.1. Characterization of AgNPs

It is important to stress that highly enriched  $^{109}\text{AgNPs}$  were synthesized by the same procedure and under the same conditions (concentrations of precursor, reducing and stabilizing agents) used to produce the corresponding AgNPs consisting of a natural isotope composition, with the exception noted in the Experimental section. Naturally occurring Ag consists of two stable isotopes,  $^{107}\text{Ag}$  and  $^{109}\text{Ag}$ , with the former slightly more abundant (51.839%) than the latter (48.161%) [41]. In order to illustrate the capability to characterize the isotopically enriched  $^{109}\text{AgNPs}$  and to evaluate the quality of the synthesized materials, results for  $^{109}\text{AgNPs}$  are directly compared to AgNPs produced using the natural isotopic ratio.

**Table 1**  
Summary of instrumental conditions and parameters used in this study.

Instrumentation			Size range characterized	
			Condition A (1–50) nm	Condition B (50–450) nm
A4F	Channel equipment	Injection volume	100 $\mu\text{L}$	100 $\mu\text{L}$
		Membrane	PES, 10 KDa	PES, 10 KDa
		Spacer	350 $\mu\text{m}$ (large width)	250 $\mu\text{m}$ (medium width)
	Flow ( $\text{mL min}^{-1}$ )	Channel flow	0.5 $\text{mL min}^{-1}$	0.5 $\text{mL min}^{-1}$
		Inject flow	0.2 $\text{mL min}^{-1}$	0.2 $\text{mL min}^{-1}$
		Focus flow	2.0 $\text{mL min}^{-1}$	2.0 $\text{mL min}^{-1}$
		Cross flow	0.8 $\text{mL min}^{-1}$	0.2 $\text{mL min}^{-1}$
		Elution step	Focus + injection	5 min
		Focus	3 min	3 min
		Elution	40 min	25 min
DAD	Wavelength	(190 to 900) nm		
	Sampling rate	0.01 s		
Light scattering	Wavelength	658 nm		
	Scattering volume	0.07 $\mu\text{L}$		
	MALS detector	90° reference angle Zimm formalism (1st order)		
	DLS detector	107° angle position Cumulants method		
ICP-MS	Nebulizer flow rate	0.16 $\text{mL min}^{-1}$		
	Sample and skimmer cones	Ni		
	RF power	1500 W		
	Plasma gas flow rate	15 $\text{L min}^{-1}$		

Fig. 1 shows 3-dimensional (3D) fractograms obtained for (a) the naturally occurring AgNP isotopic composition and (b) the enriched  $^{109}\text{Ag}$ NPs, both analyzed at a concentration of  $0.006 \text{ g L}^{-1}$ . To obtain Fig. 1, the UV–vis spectra were measured in real time using the on-line DAD as a function of time during elution. The retention time,  $t_R$ , is by convention measured relative to the so-called void peak as the point of reference, but in Fig. 1 the time axis has not been corrected; therefore, sample elution actually begins at 11 min in these fractograms. The principal 3D retention peak for the AgNPs with a natural isotope ratio is centered at 19 min with a width from roughly (15–24) min (Fig. 1a). The UV–vis absorbance axis indicates a strong SPR band centered at 389 nm, with a width from (330 to 440) nm; these results are consistent with the UV–vis spectra obtained on the stock suspension using a batch mode UV–vis spectrometer (see SI, Fig. S2) and with previously reported SPR results for AgNPs of this approximate size [42–44]. For  $^{109}\text{Ag}$ NPs, the 3D retention peak is centered at 22 min with a width from (18 to 28) min. The SPR band for the AgNPs is red shifted to 398 nm and exhibits a broad shoulder toward longer wavelengths. These results are indicative of a slightly larger primary size for  $^{109}\text{Ag}$ NPs compared with the natural isotope AgNP population (indicated by the red shift), and the presence of agglomerates in the  $^{109}\text{Ag}$ NP population (indicated by the shoulder). These differences are most likely an artifact of converting the  $^{109}\text{Ag}$  metal to the nitrate salt using nitric acid; optimization of this procedure would likely yield agglomerate free particles, but this was not the focus of the present work.

Fig. 2 compares representative 2D A4F fractograms for the natural and isotopically enriched AgNPs shown in Fig. 1. Here the elution traces include MALS (scattering angle of 90°) and UV–vis (tuned to the SPR band at 400 nm). On-line DLS data ( $r_H$ ) are superimposed on these traces (solid circles) and can be compared to  $r_H$  derived from the calibrated retention time (upper x-axis). Theoretically, the two measurements of  $r_H$  should coincide, however they can differ somewhat due to various factors that are instrument and technique dependent, and difficult to quantify.

Results confirm that the primary AgNPs (both natural and isotopically enriched) are very close in size ( $r_H$  centered at  $10.8 \text{ nm} \pm 0.4 \text{ nm}$ ), but that the  $^{109}\text{Ag}$ NPs contain more

agglomerates relative to the natural isotopic AgNPs. The difference in the maximum peak position between UV–vis and MALS is due to the different principles of detection associated with each trace. Specifically, the light scattering detector depends on both size and concentration (intensity scales with  $r^6$ ,  $r$  being the generic radius of the particle), while the UV–vis trace depends only on the AgNP concentration. These results demonstrate the advantage of coupling A4F separation with both absorbance and scattering detectors, in order to have a more complete assessment of the particle state; note that the MALS trace indicates the presence of a small population of agglomerates, although this population is invisible to the DAD due to the low concentration and SPR shift. The characteristic size of these two samples determined by the A4F-multi detector approach corresponds to the size obtained by DLS in batch mode for the stock solution (i.e., without fractionation); the  $r_H$  distribution is presented in the SI (see Fig. S3).

The resulting information is useful for determining the influence of various environmental, biochemical and physico-chemical factors on the final size distribution, composition, and agglomeration state for AgNPs, which will be discussed further below.

Despite the richness of data provided by A4F coupled to multiple optical detection modalities, the ability to identify and quantify AgNPs in complex media (environmental and biological) is still limited by the capacity to track specific particles of interest amongst a multitude of interfering species, including naturally occurring and anthropogenic colloidal Ag, which can result directly from the presence of dissolved Ag ions in natural waters. [45]. With the methodology described in the present work, we demonstrate the benefit of coupling A4F to ICP-MS in order to discriminate isotopic compositions (or ratios) for AgNPs arising from different sources. Fig. 3 shows fractograms obtained by A4F-ICP-MS in which  $^{107}\text{Ag}$ ,  $^{109}\text{Ag}$ , and the ratio  $[^{109}\text{Ag}]/[^{107}\text{Ag}]$  are traced following an ICP-MS calibration for Ag quantification (see SI for details). For natural isotopic AgNPs, the ICP-MS signals for  $^{107}\text{Ag}$  and  $^{109}\text{Ag}$  align closely with the primary MALS peak maximum and width, although they are reversed relative to their natural abundances (i.e.,  $^{109}\text{Ag}$  is just above  $^{107}\text{Ag}$ , rather than the reverse). This reversal is an artifact due to the slightly higher instrumental background for  $^{109}\text{Ag}$ ; the source of this higher background may be due to different factors,

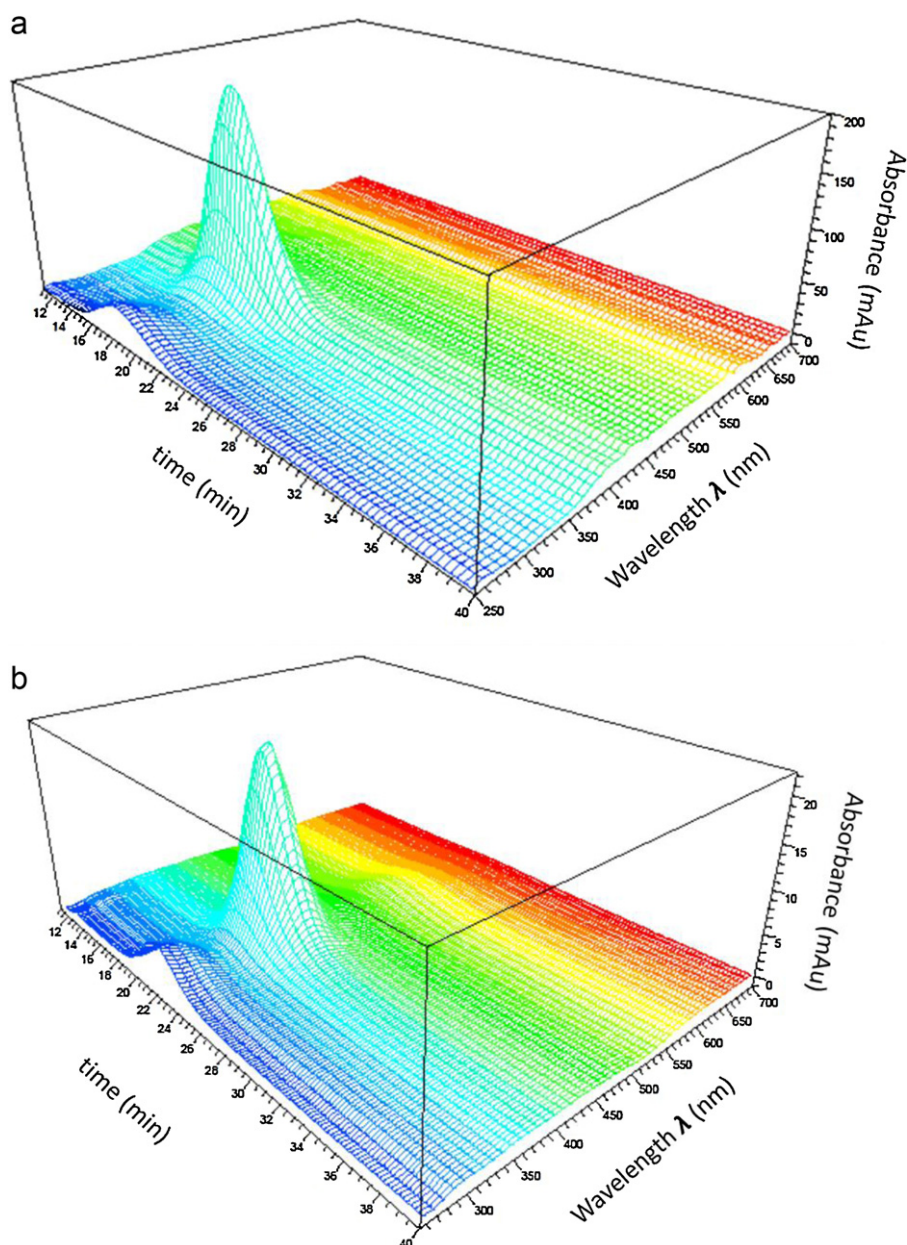


**Fig. 1.** Three dimensional fractograms based on UV-vis spectral absorbance for (a) AgNPs with the natural isotopic ratio and (b) isotopically enriched  $^{109}\text{Ag}$ NPs. The time axis includes the focus and injection steps, with sample elution starting at 11 min.

such as mass specific interferences, but is beyond the scope of the present work and not significant for our present purposes. For the isotopically enriched  $^{109}\text{Ag}$ NPs, as expected the corresponding  $^{109}\text{Ag}$  mass signal is clearly dominant compared to the barely perceptible  $^{107}\text{Ag}$  signal. The ICP-MS signals for both natural isotopic AgNPs and  $^{109}\text{Ag}$ NPs correspond in terms of their observed elution time range. The shift in elution time between UV-vis (400 nm) and MALS signals allows one to discriminate between AgNPs individually dispersed and their agglomerates. Although isotopically pure  $^{109}\text{Ag}$ NPs and their natural AgNP analogs of the same or similar size would be expected to coelute, by plotting the ratio  $[^{109}\text{Ag}]/[^{107}\text{Ag}]$  as a function of elution time (Fig. 3c), the specificity of the method toward different stable isotopic formulations and the possibility to discriminate between them is clearly demonstrated; in the current study, natural and isotopically modified AgNPs are examined separately.

In summary, the isotopically enriched or modified AgNPs exhibit similar optical and physical properties compared with AgNPs with

a natural isotopic ratio, but yield a specific isotopic signature that can be detected and quantified. This signature characterization was realized in situ and in real time, along with the size and optical properties using the hyphenated method A4F-DAD-MALS-DLS-ICP-MS. The application of this method to environmental and biological media can be relevant in order to determine their behavior and reactivity.

### 3.2. Tracing AgNPs in an environmental matrix

#### 3.2.1. AgNP interaction with natural organic matter

As an application of this methodology, we investigated the detection and characterization of isotopically enriched  $^{109}\text{Ag}$ NPs in an environmental matrix consisting of standard estuarine sediment and natural organic matter (NOM) in an aqueous suspension. This matrix presents a number of measurement challenges due to its complex composition as well as the potential interaction of the target AgNPs with both particulate and dissolved species. In order

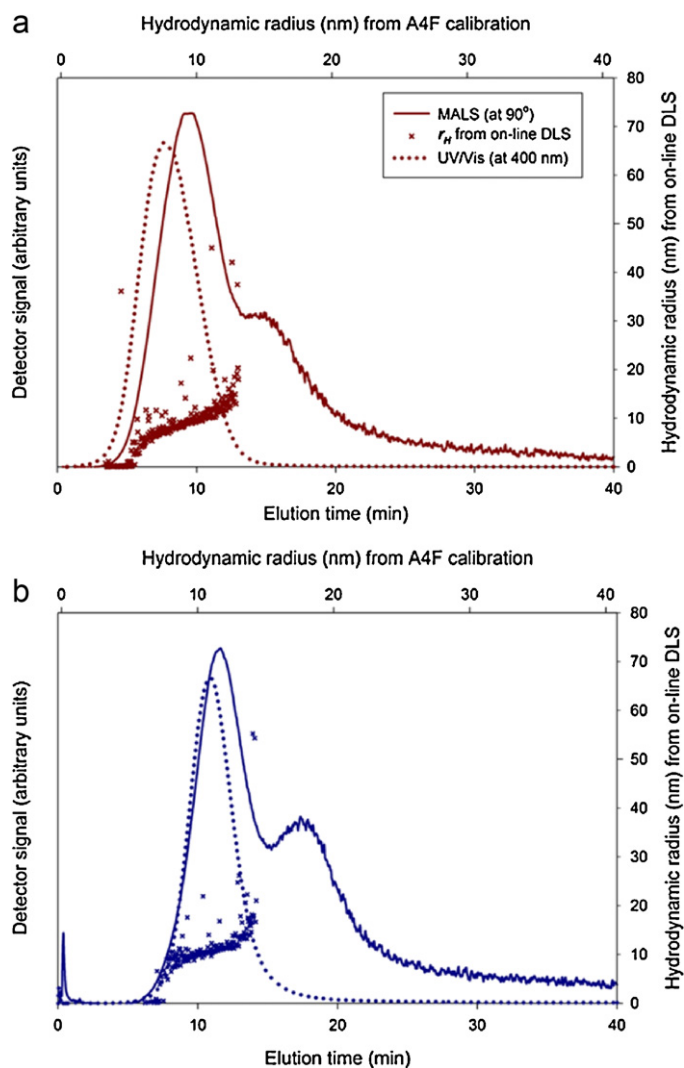


**Fig. 2.** Fractograms for (a) natural isotopic ratio AgNPs and (b) enriched  $^{109}\text{Ag}$ NPs, showing the DAD trace at 400 nm (dotted line), scattering intensity trace (solid line) measured at  $90^\circ$  and  $r_H$  (filled circles) measured by on-line DLS at a scattering angle of  $117^\circ$ . The upper x-axis of each graph corresponds to  $r_H$  determined from the retention time calibration (see SI, Fig. S1). For the conditions of fractionation see Table 1.

to replicate their likely state in natural waters, the  $^{109}\text{Ag}$ NPs were initially exposed to NOM in the form of Suwannee River humic (HA) or fulvic (FA) acid standards. The concentration of Ag in these solutions remained relatively unchanged:  $0.0054 \text{ g L}^{-1}$  and  $0.0052 \text{ g L}^{-1}$  for HA and FA coated  $^{109}\text{Ag}$ NPs, respectively, by taking account of the slight dilution during the ligand exchange process. Fig. 4a presents 3D absorbance fractograms and Fig. 4c shows the corresponding 2D light scattering fractograms ( $r_G$  and  $r_H$ ) obtained by A4F-DAD-MALS-DLS for  $^{109}\text{Ag}$ NPs exposed to HA (referred to as  $^{109}\text{AgNP-HA}$ ). The 3D fractograms for  $^{109}\text{AgNP-HA}$  are consistent with the native  $^{109}\text{Ag}$ NPs, considering the SPR maximum and the retention time for primary particles. This indicates that HA induces no significant change in the final optical and dispersion properties. Similarly, Fig. 4c indicates that the maximum for the primary  $^{109}\text{Ag}$ NPs exposed to HA corresponds with the result obtained for the native citrate stabilized  $^{109}\text{Ag}$ NPs, and that the size results are also in line with the previous obtained results. Additionally, a decrease intensity for the agglomeration peak ( $\approx 18 \text{ min}$ ) located at a longer retention time (compare Figs. 3b and 4c), suggests one of two possible scenarios: either HA aids in the dispersal of agglomerates or the existing agglomerates form even larger structures in

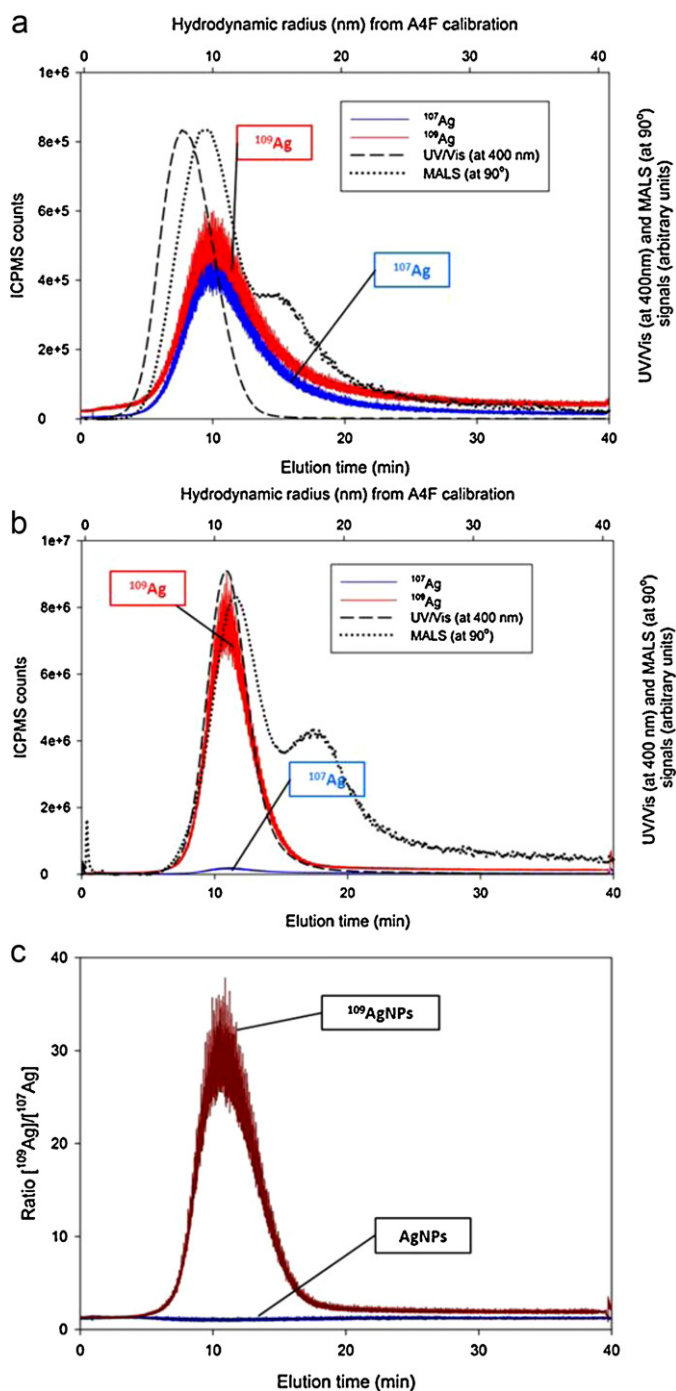


**Fig. 3.** A4F fractograms showing  $^{107}\text{Ag}$  and  $^{109}\text{Ag}$  mass traces obtained in coupled mode using ICP-MS (fractionation condition A, see Table 1) for (a) natural isotopic AgNPs and (b) isotopically enriched  $^{109}\text{Ag}$ NPs. Fractogram tracing the measured isotopic mass ratio  $^{109}\text{Ag}/^{107}\text{Ag}$  is presented in (c) for each AgNP population. The  $^{109}\text{Ag}$  background is slightly higher, accounting for the apparent reversal in isotopic ratio for the natural composition in (a). In (a) and (b) the MALS (scattering intensity at  $90^\circ$ ) and UV-vis (400 nm) traces are overlaid for comparison.

the presence of HA that are not eluted within the time frame of this experiment.

Surprisingly, the secondary MALS peak attributed to agglomerates above is not accompanied by significant optical absorption over the measured wavelength range (see Fig. 4(a) and (c)). Similarly, in Fig. 2(a) and (b), the on-line DLS detector fails to provide a precise size determination for the agglomerate population. These results are due to a combination of factors including the small

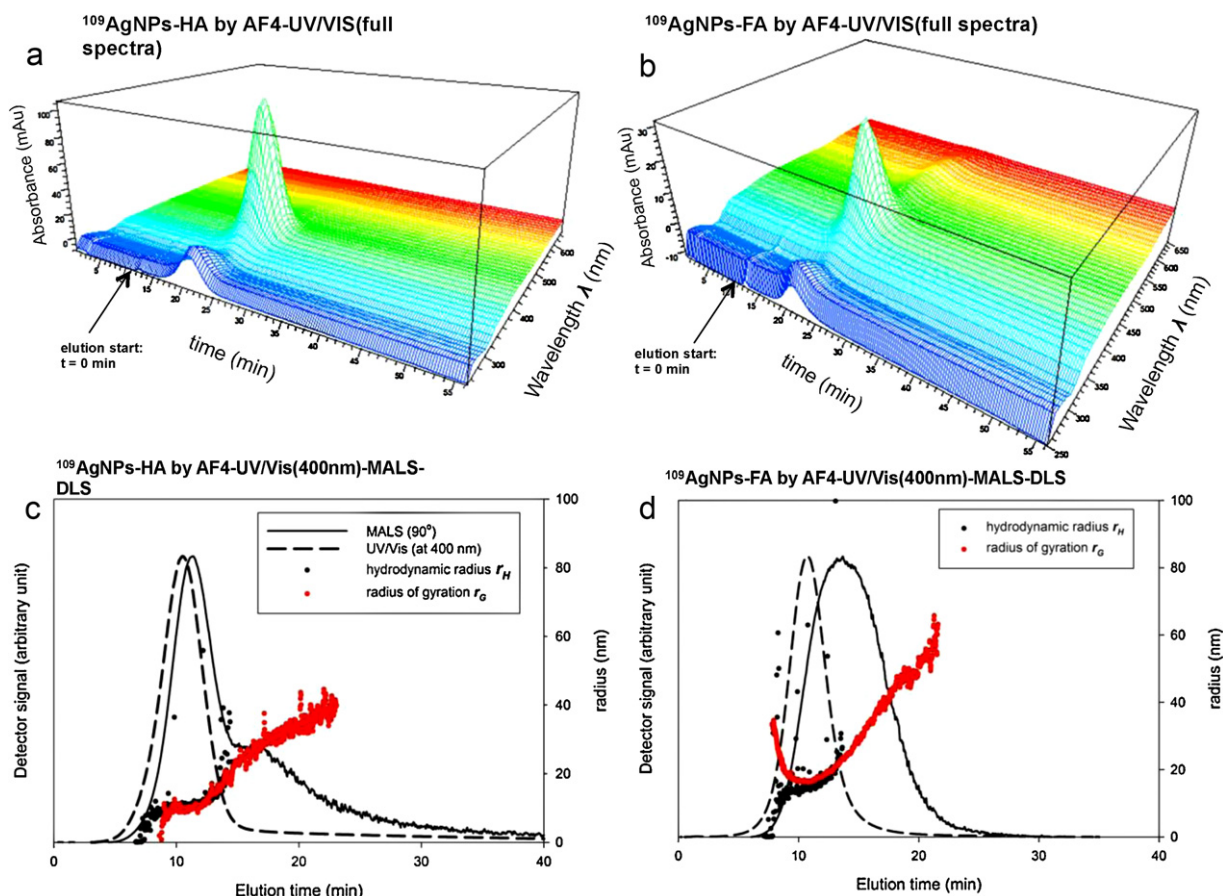


**Fig. 4.** Fractograms for  $^{109}\text{AgNP-HA}$  and  $^{109}\text{AgNP-FA}$ . (a) and (b) 3D absorbance fractograms obtained by A4F-DAD (full spectra, scan rate 0.01 s); (c) and (d) 2D fractograms showing light scattering trace (measured at  $90^\circ$ , solid line) and UV-vis absorbance trace (measured at 400 nm, dashed line) obtained by A4F-DAD-MALS, and overlaid with the  $r_G$  (red dot) and  $r_H$  (black dot) as a function of the elution time. All fractograms were realized with the A4F condition A (see Table 1). The arrow on the time axis in the 3D fractograms indicates the start of sample elution at 11 min. (For interpretation of the references to color in this figure legend, the reader is referred to the web version of the article.)

number of agglomerates present in the band, the decrease in SPR absorbance resulting from particle contact, the small scattering volume, the short residence time of the particles in the beam, and the longer correlation times required to capture the correlation decay for these larger particles. On the other hand, the on-line DLS results for the primary AgNPs match closely with the radius of gyration obtained from analysis of the MALS data using the Zimm plot approach; that is, the smaller primary particles diffuse rapidly relative to their residence time in the beam, and are therefore amenable to on-line DLS analysis.

Corresponding results for FA exposed  $^{109}\text{AgNPs}$  ( $^{109}\text{AgNP-FA}$ ) are presented in the right hand panels of Fig. 4. The 3D fractograms show a substantial alteration of the SPR absorbance pattern, leading to an extended shoulder at longer wavelengths, a band maximum red-shifted to 450 nm and another band appearing at longer wavelengths (>450 nm) at slightly higher retention time. This result clearly indicates that, rather than stabilizing AgNPs, FA induces the formation of agglomerates. This is further evidenced by the single broad MALS peak in the 2D fractogram for  $^{109}\text{AgNP-FA}$  shown in Fig. 4b (right side) relative to the native  $^{109}\text{AgNPs}$  in Fig. 2b (left side).

According to this observation and considering the variation of the  $r_H$  and  $r_G$ , this indicates that the particle size associated with both the primary SPR band and the broad shoulder (associated with the agglomerates) increase in the presence of FA. Additionally, the ratio  $^{109}\text{Ag}/^{107}\text{Ag}$  as a function of the elution time presented in Fig. 5, shows the same signal retention time range as the fractograms traced by MALS, and therefore validates the

coupling between A4F and the various detectors as well as the information obtained. Moreover, the ratio  $^{109}\text{Ag}/^{107}\text{Ag}$  remains constant even though the particles are slightly diluted during the ligand exchange with HA or FA solutions.

The difference in observed behavior of  $^{109}\text{AgNPs}$  exposed to HA and FA can be attributed to differences in the chemical composition of each NOM fraction. HA is composed of macromolecules

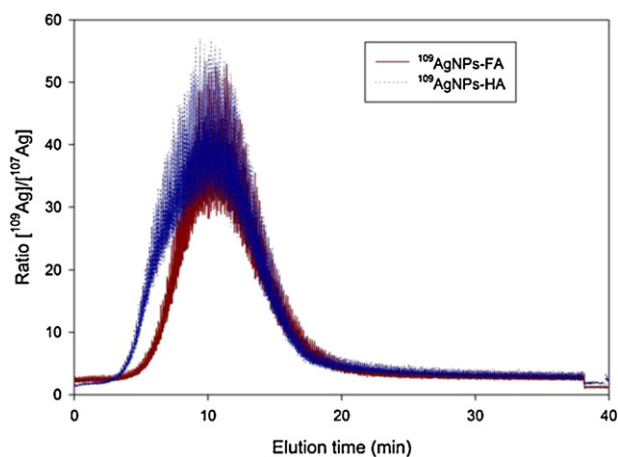


**Fig. 5.** Comparison of fractograms obtained by A4F-ICP-MS and presented as the ratio  $^{109}\text{Ag}/^{107}\text{Ag}$  for HA and FA treated isotopically enriched  $^{109}\text{AgNPs}$ , realized with A4F fractionation condition A (Table 1).

with a molar mass ranging from about (10 to 200) kDa, while the molar mass of FA ranges from about (1 to 8) kDa [46,47]. The higher molar mass most likely contributes to increased stability via a more extensive surface corona; FA has been described as a colloidal phase, suggesting it is more compact and less polymeric in nature. Although the phenolic content of the Suwannee River derived HA and FA used in this study is statistically indistinguishable, FA has a substantially higher carboxylic sites [48]. These factors likely play a significant role in differentiating the behavior of HA and FA treated AgNPs, but the inherent structural complexity of NOM makes it difficult to draw clear conclusions.

### 3.2.2. $^{109}\text{AgNP}$ tracking in estuarine matrix leachate

The NOM treated  $^{109}\text{AgNP}$  suspensions were then mixed into the standard estuarine sediment with an equivalent volume of deionized water to obtain solutions S1 (with  $^{109}\text{AgNP-HA}$ ) and S2 (with  $^{109}\text{AgNP-FA}$ ). After incubation, the leachates from S1 and S2 were obtained. In order to determine if any primary AgNPs remain free in the leachate solutions, A4F condition A (for particles <50 nm) was initially applied. The A4F-DAD-ICP-MS (with DAD tuned to 254 nm) fractogram obtained for the S1 leachate is presented in Fig. S3 in the SI. The results show that the isotopic mass ratio  $[^{109}\text{Ag}]/[^{107}\text{Ag}]$  remains constant at background level even as a strong UV absorbance signal is detected at  $t_R = 2.3$  min. Furthermore, no absorbance was detected at 400 nm (the AgNP SPR band) at the retention time corresponding to the peak in the UV absorbance at 254 nm, suggesting that this peak is not associated with  $^{109}\text{AgNPs}$ , but consists of other HA containing components (aromatic compounds absorb strongly at 254 nm). Virtually identical results were observed for leachate S2 (not shown).

A4F separation was performed to measure particle sizes from (50 to 400) nm using A4F condition B given in Table 1; a typical fractogram is presented in Fig. S4 of the SI. The calibration of the A4F method for this size range was realized using both standard polystyrene latex particles and commercial AgNPs (see SI, Fig. S1b), since the environmental matrix contains a wide range of organic and inorganic constituents. This linear calibration between  $t_R$  and  $r_H$  (measured by on-line DLS) allow us to determine the size of the analytes directly from the A4F measurement. In addition, commercial PVP-coated AgNPs were analyzed under the same fractionation condition. It appears that the  $r_H$  obtained for the PVP-AgNPs using the calibration realized with latex nanosphere standards accurately reflects the expected size. This result indicates that the A4F fractionation method for AgNPs in this size range does not depend strongly on the material nature, but principally on the analyte dimensional properties (size and spherical shape). So, the calibration between  $r_H$  and retention time (Eq. (2)) can be used to directly convert time to  $r_H$  for AgNPs and other components. The result obtained does not correspond to a size distribution, as it includes also band broadening effects; on the other hand, the trace provides information on the mean  $r_H$  for an eluting component. It is important to note that the on-line DLS detector cannot yield accurate size data in this mode, due to the small scattering volume, short residence time and high polydispersity of the sample.

Fig. 6 presents the fractograms obtained using traces from three detectors (DAD tuned to 254 nm, MALS at  $90^\circ$ , and ICP-MS) for the S1 and S2 leachates. The final concentrations of total  $^{109}\text{Ag}$  in these solutions were not measured in batch mode. Instead we integrated the peaks in the fractograms in order to evaluate the quantity of  $^{109}\text{Ag}$  and we then traced the ratio  $^{109}\text{Ag}/^{107}\text{Ag}$ . Using this approach, we measured  $23.2 \pm 0.1 \mu\text{g L}^{-1}$  and  $48.6 \pm 0.2 \mu\text{g L}^{-1}$  of  $^{109}\text{Ag}$  in S1 and S2 respectively. Generally, it appears that the calibration obtained with the different standards (to convert  $t_R$  to  $r_H$ ) is consistent with the variation of  $r_G$  calculated from the MALS data, essentially validating the fractionation and calibration methods developed for this size range. Additionally, before the analysis

of the two leachates, the signal obtained for the control leachate S0 was determined for all detectors. In the case of ICP-MS, the background ratio  $[^{109}\text{Ag}]/[^{107}\text{Ag}]$  was  $1.14 \pm 0.02$  (see SI, Fig. S4), which is slightly higher than the expected ratio for naturally occurring isotopes (0.93), again due to the slightly higher instrument background observed for  $^{109}\text{Ag}$  in all experiments.

Concerning leachate S1 that was realized by adding  $^{109}\text{AgNP-HA}$  to the estuarine sediment, the predominant MALS signal (Fig. 6a) corresponds to particles with radii ranging from about (40 to 120) nm. The isotopic mass ratio signal corresponding to the  $^{109}\text{AgNPs}$  incubated in the sediment suspension reaches its maximum at a retention time slightly shifted (toward faster elution) from the MALS peak; this shift may indicate that  $^{109}\text{AgNPs}$  remain to some degree hydrodynamically independent from the larger sediment particles and elute separately, or it may simply be a reflection of the strong size dependence for static light scattering (an effect that shifts the MALS peak toward larger sizes in a polydisperse population). For solution S2, a similar observation can be made, except that in this case a second DAD peak centered at  $t_R = 5$  min (Fig. 6b), absent in Fig. 6a, aligns closely with the isotopic ratio peak associated with the incubated  $^{109}\text{AgNPs}$ . Taken as a whole, the results here suggest that both of the NOM-treated  $^{109}\text{AgNPs}$  associate with natural colloidal matter in the sediment, as characterized by the size range obtained by MALS and A4F calibration in the leachates. However, the principal aim of this study was not to characterize the nature of these interactions, but rather to demonstrate proof-of-principle for methodology to monitor behavior of manufactured AgNPs in a complex environmental medium. Even so, the A4F results clearly show that all detector signals (i.e., MALS, DAD, ICP-MS) are substantially higher for S2 relative to S1 (see Fig. 6). This suggests that the larger  $^{109}\text{AgNP-FA}$  particles interact to a lesser degree with the sediment than the smaller  $^{109}\text{AgNP-HA}$  particles. Alternatively, FA itself may somehow directly mitigate these interactions. Either way, the end result is that a greater number of the tracer  $^{109}\text{AgNPs}$  end up in the leachate when treated with FA than when treated with HA.

The ratio  $[^{109}\text{Ag}]/[^{107}\text{Ag}]$  obtained in the leachate solutions decreases substantially compared to the ratio obtained for  $^{109}\text{AgNP-FA}$  and  $^{109}\text{AgNP-HA}$  (see Fig. 5). The decrease of the ratio can only be explained by an isotopic dilution, which suggests two possibilities:

1. Ag ions contained in the estuarine sediment are adsorbed or in some way associated with the synthetic forms of  $^{109}\text{AgNPs}$  characterized in Fig. 6. The sediment SRM is stated to contain  $<300 \mu\text{g L}^{-1}$  Ag in an unknown form [39]. Nevertheless the ICP-MS results for the colloidal phase eluted from leachates S1, S2 and S0 (SI, Fig. S4) all indicate that  $^{107}\text{Ag}$  is at background levels. Additionally the off-line ICP-MS quantification of leachate S0 yielded only trace levels of Ag ( $<1 \mu\text{g L}^{-1}$ ), which are too low to produce a significant isotopic dilution of  $^{109}\text{Ag}$  in the leachate.
2. A substantial fraction of the tracer AgNPs interact with the estuarine sediment, producing a partition of the particles into two phases: a small quantity remains in the liquid phase existing in agglomerated or colloid-associated form, and a second predominant quantity remains trapped in the sediment. This can explain the decrease in the signal for  $^{109}\text{Ag}$  relative to  $^{107}\text{Ag}$  in the leachate. It should be noted that the latter mass signal is always consistently low and at background levels for this set of experiments, so any decrease in  $^{109}\text{AgNPs}$  in the sample will result in a decrease in the  $^{109}\text{Ag}$  ICP-MS signal with the  $^{107}\text{Ag}$  signal appearing relatively unchanged.

So, of these two possibilities, the second one appears to be the most likely explanation for the decrease in the  $[^{109}\text{Ag}]/[^{107}\text{Ag}]$  ratio in leachate solutions.

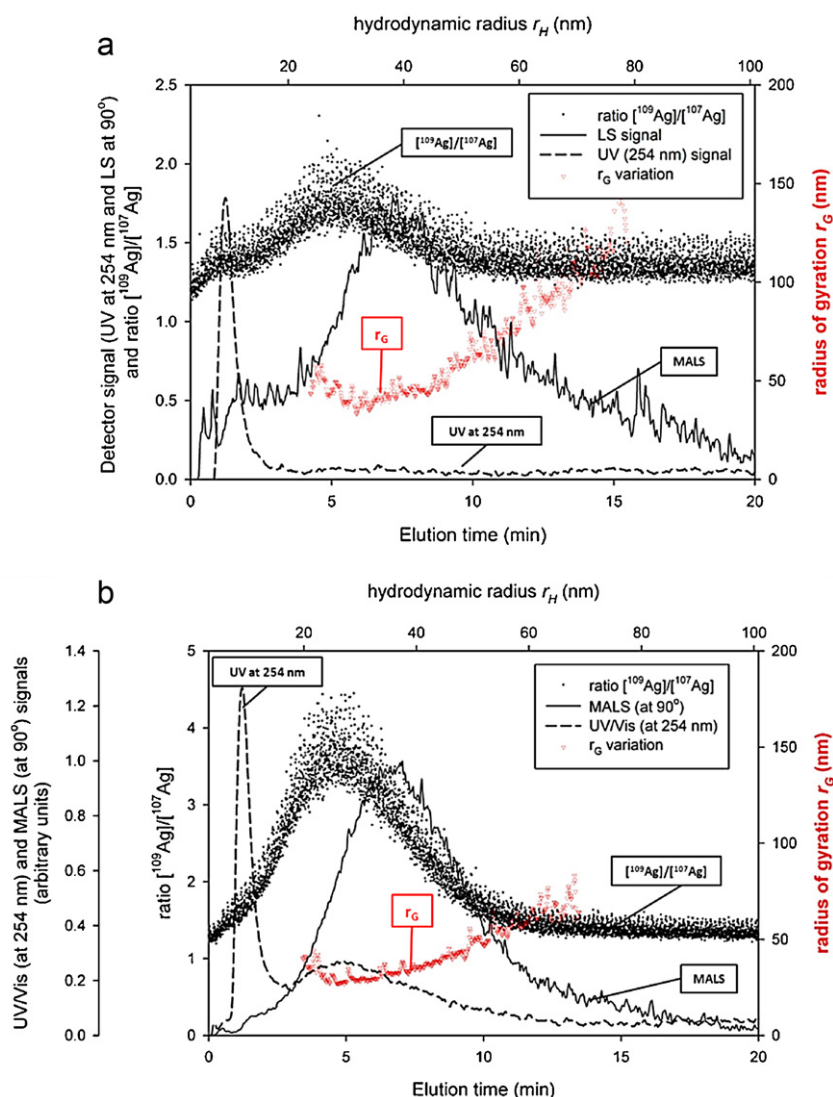


**Fig. 6.** Fractograms with the MALS signal (full line), UV signal tuned at 254 nm (dashed line), the ratio  $[^{109}\text{Ag}]/[^{107}\text{Ag}]$  obtained by the ICP-MS (dotted trace), and the variation of the radius of gyration obtained by analysis of MALS (open triangles), versus the elution time and the  $r_H$  (determined by A4F calibration using polystyrene latex nanosphere standards) for (a) leachate S1 using  $^{109}\text{AgNP-HA}$  and (b) leachate S2 using  $^{109}\text{AgNP-FA}$ . All fractograms were realized with the A4F condition B described in Table 1.

Nevertheless, for the same quantity of NOM, even if a substantial decrease in the ratio was observed, leachate S1 containing  $^{109}\text{AgNP-HA}$  indicates a higher level of isotopic dilution. This means that the  $^{109}\text{AgNP-HA}$  particles must interact to a larger extent with the solid phase in the sediment. Since the original size of  $^{109}\text{AgNP-HA}$  is smaller than  $^{109}\text{AgNP-FA}$ , it could be possible to explain this observation by imagining that  $^{109}\text{AgNP-HA}$  has greater diffusivity in the sediment phase and can therefore interact more efficiently with species contained in the sediment.

The most salient feature of these results is the clear difference between the behaviors of HA- and FA-treated AgNPs when they are mixed into an estuarine sediment suspension. Although the differences require further investigation to fully understand the underlying mechanisms and to probe the resulting environmental repercussions, the methodology described here clearly demonstrates great potential for this approach, in terms of specificity, sensitivity and quantitative analysis.

#### 4. Conclusions

The purpose of this work was to develop and, to the extent possible, validate a new methodology based on asymmetric-flow field

flow fractionation coupled to multi-mode detection that simultaneously yields information related to the physical, compositional and optical properties of AgNPs, and to combine this instrumental approach with the use of stable isotopes in order to better assess the environmental or biological fate of such particles. By coupling ICP-MS to A4F, we demonstrated that the isotopic signature of AgNPs can be directly determined (without pre-digestion) and used to differentiate between isotopically enriched tracers and naturally occurring or anthropogenic species. This methodology was demonstrated using an estuarine sediment reference material, by doping the suspension with a quantity of isotopically enriched  $^{109}\text{AgNPs}$  pretreated with standard Suwannee River humic or fulvic acids. The results indicate that humic and fulvic acid coated particles interact differently with the estuarine sediment components, and yield leachates that have characteristically different elution and isotopic signatures. The methodology described here promises new opportunities to monitor and study the fate and transformations of AgNPs in complex and relevant environmental or biological matrices. While this study demonstrates proof of principle and focuses on the interactions of nanoscale Ag particles, the approach can be extended to examine both soluble and particulate phases and their transformations. At the same time, this methodology can

be extrapolated to other nanoparticle systems, particularly metal containing species with available stable isotopes.

### Acknowledgements

The authors thank Dr. Karen Murphy of NIST for kindly providing a sample of SRM 1646a. J.G. thanks Dr. Rob MacCuspie of NIST for providing guidance on implementing the AgNP synthesis procedure adopted for this study, and for insightful technical discussions.

### Appendix A. Supplementary data

Supplementary data associated with this article can be found, in the online version, at <http://dx.doi.org/10.1016/j.aca.2012.11.060>.

### References

- [1] X. Chen, H.J. Schluesener, *Toxicol. Lett.* 176 (2008) 1.
- [2] J. Fabrega, R. Zhang, J.C. Renshaw, W.-T. Liu, J.R. Lead, *Environ. Sci. Technol.* 43 (2009) 7285.
- [3] V. Gopinath, D. MubarakAli, S. Priyadarshini, N.M. Priyadarshini, N. Thajuddin, P. Velusamy, *Colloids Surf. B: Biointerfaces* 96 (2012) 69.
- [4] V.K. Sharma, R.A. Yngard, Y. Lin, *Adv. Colloid Interface Sci.* 145 (2009) 83.
- [5] M. Rai, A. Yadav, A. Gade, *Biotechnol. Adv.* 27 (2009) 76.
- [6] L.S. Nair, C.T. Laurencin, *J. Biomed. Nanotechnol.* 3 (2007) 301.
- [7] S. Shrivastava, T. Bera, A. Roy, G. Singh, P. Ramachandrarao, D. Dash, *Nanotechnology* 18 (2007) 225103.
- [8] M. Ahamed, M.S. AlSalhi, M.K.J. Siddiqui, *Clin. Chim. Acta* 411 (2010) 1841.
- [9] S. Galdiero, A. Falanga, M. Vitiello, M. Cantisani, V. Marra, M. Galdiero, *Molecules* 16 (2011) 8894.
- [10] P. Irwin, J. Martin, L.-H. Nguyen, Y. He, A. Gehring, C.-Y. Chen, *J. Nanobiotechnol.* 8 (2010) 34.
- [11] Our Silver-Coated Future | OnEarth Magazine. <http://www.onearth.org/article/our-silver-coated-future>
- [12] Silver Nanotechnology in Commercial Products, Wilson Center data base. <http://www.nanotechproject.org/inventories/silver/>
- [13] V.L. Colvin, *Nat. Biotechnol.* 21 (2003) 1166.
- [14] K.A.D. Guzmán, M.R. Taylor, J.F. Banfield, *Nanomed. -Nanotechnol.* 8 (2006) 1401.
- [15] Y. Ju-Nam, J.R. Lead, *Sci. Total Environ.* 400 (2008) 396.
- [16] R.D. Handy, R. Owen, E. Valsami-Jones, *Ecotoxicology* 17 (2008) 315.
- [17] T.M. Tolaymat, A.M. El Badawy, A. Genaidy, K.G. Scheckel, T.P. Luxton, M. Suidan, *Sci. Total Environ.* 408 (2010) 999.
- [18] A.K. Suresh, D.A. Pelletier, W. Wang, J.L. Morrell-Falvey, B. Gu, M.J. Doktycz, *Langmuir* 28 (2012) 2727.
- [19] B. Nowack, T.D. Bucheli, *Environ. Pollut.* 150 (2007) 5.
- [20] C. Levard, E.M. Hotze, G.V. Lowry, G.E. Brown, *Environ. Sci. Technol.* 46 (2012) 6900.
- [21] J.M. Zook, S.E. Long, D. Cleveland, C.L.A. Geronimo, R.I. MacCuspie, *Anal. Bioanal. Chem.* 401 (2011) 1993.
- [22] R.I. MacCuspie, K. Rogers, M. Patra, Z. Suo, A.J. Allen, M.N. Martin, V.A. Hackley, *J. Environ. Monit.* 13 (2011) 1212.
- [23] J.-F. Liu, S.-J. Yu, Y.-G. Yin, J.-B. Chao, *TrAC – Trends Anal. Chem.* 33 (2012) 95.
- [24] K. Tiede, A. Boxall, S. Tear, J. Lewis, H. David, M. Hasselov, *Food Add. Contam. A* 25 (2008) 795.
- [25] B.F. da Silva, S. Pérez, P. Gardinalli, R.K. Singhal, A.A. Mozeto, D. Barceló, *TrAC Trends Anal. Chem.* 30 (2011) 528.
- [26] M. Hasselöv, J.W. Readman, J.F. Ranville, K. Tiede, *Ecotoxicology* 17 (2008) 344.
- [27] R.I. MacCuspie, A.J. Allen, V.A. Hackley, *Nanotoxicology* 5 (2011) 140.
- [28] A.R. Poda, A.J. Bednar, A.J. Kennedy, A. Harmon, M. Hull, D.M. Mitrano, J.F. Ranville, J. Steevens, *J. Chromatogr. A* 1218 (2011) 4219.
- [29] E. Bolea, J. Jiménez-Lamana, F. Laborda, J.R. Castillo, *Anal. Bioanal. Chem.* 401 (2011) 2723.
- [30] M.E. Hoque, K. Khosravi, K. Newman, C.D. Metcalfe, *J. Chromatogr. A* 1233 (2012) 109.
- [31] H. Hagendorfer, R. Kaegi, M. Parlinska, B. Sinnet, C. Ludwig, A. Ulrich, *Anal. Chem.* 84 (2012) 2678.
- [32] B. Stolpe, M. Hasselöv, K. Andersson, D.R. Turner, *Anal. Chim. Acta* 535 (2005) 109.
- [33] M.E. Schimpf, K. Caldwell, J.C. Giddings, *Field Flow Fractionation Handbook*, Wiley-IEEE, New York, 2000.
- [34] G. Lespes, J. Gigault, *Anal. Chim. Acta* 692 (2011) 26.
- [35] D.-H. Tsai, T.J. Cho, F.W. Delrio, J. Taurozzi, M.R. Zachariah, V.A. Hackley, *J. Am. Chem. Soc.* 133 (2011) 8884.
- [36] M. Baalousha, B. Stolpe, J.R. Lead, *J. Chromatogr. A* 1218 (2011) 4078.
- [37] V. Amendola, O.M. Bakr, F. Stellacci, *Plasmonics* 5 (2010) 85.
- [38] S. Dubascoux, I. Le Hécho, M. Hasselöv, F. Von Der Kammer, M. Potin Gautier, G. Lespes, *J. Anal. At. Spectrom.* 25 (2010) 613.
- [39] Standard Reference Material 1646A, Certificate of Analysis, National Institute of Standards and Technology. [http://www-s.nist.gov/srmors/view\\_cert.cfm?srml1646A](http://www-s.nist.gov/srmors/view_cert.cfm?srml1646A), 2004.
- [40] R.I. MacCuspie, *J. Nanopart. Res.* 13 (2011) 2893.
- [41] J.R. de Laeter, J.K. Böhlke, P. De Bièvre, H. Hidaka, H.S. Peiser, K.J.R. Rosman, P.D.P. Taylor, *Pure Appl. Chem.* 75 (2003) 683.
- [42] C.H. Munro, W.E. Smith, M. Garner, J. Clarkson, P.C. White, *Langmuir* 11 (1995) 3712.
- [43] S.L. Chinnapongse, R.I. MacCuspie, V.A. Hackley, *Sci. Total Environ.* 409 (2011) 2443.
- [44] J.M. Zook, V. Rastogi, R.I. MacCuspie, A.M. Keene, J. Fagan, *ACS Nano* 5 (2011) 8070.
- [45] N. Akaighe, R.I. MacCuspie, D.A. Navarro, D.S. Aga, S. Banerjee, M. Sohn, V.K. Sharma, *Environ. Sci. Technol.* 45 (2011) 3895.
- [46] Y.-P. Chin, G. Aiken, E. O'Loughlin, *Environ. Sci. Technol.* 28 (1994) 1853.
- [47] F. Laborda, E. Bolea, M.P. Górriz, M.P. Martín-Ruiz, S. Ruiz-Beguera, J.R. Castillo, *Anal. Chim. Acta* 606 (2008) 1.
- [48] J.D. Ritchie, E.M. Perdue, *Geochim. Cosmochim. Acta* 67 (2003) 85.